

Theory for superconductivity in alkali chromium arsenides $A_2Cr_3As_3$ ($A=K,Rb,Cs$)

Yi Zhou,^{1,2} Chao Cao,³ and Fu-Chun Zhang^{1,2}

¹Department of Physics, Zhejiang University, Hangzhou 310027, China

²Collaborative Innovation Center of Advanced Microstructures, Nanjing 210093, China

³Department of Physics, Hangzhou Normal University, Hangzhou 310036, China

(Dated: February 13, 2017)

We propose an extended Hubbard model with three molecular orbitals on a hexagonal lattice with D_{3h} symmetry to study recently discovered superconductivity in $A_2Cr_3As_3$ ($A=K,Rb,Cs$). Effective pairing interactions from paramagnon fluctuations are derived within the random phase approximation, and are found to be most attractive in spin triplet channels. At small Hubbard U and moderate Hund's coupling, the pairing arises from 3-dimensional (3D) γ band and has a spatial symmetry $f_{y(3x^2-y^2)}$, which gives line nodes in the gap function. At large U , a fully gapped p -wave state, $p_z \hat{z}$ dominates at the quasi-1D α -band.

PACS numbers: 74.20.-z; 74.20.Mn; 74.20.Rp; 74.70.-b

Recently, CrAs based superconductors have attracted much attention. CrAs itself is a 3D antiferromagnet (AFM), which becomes superconducting (SC) under modest pressure with $T_c \sim 2K$ ¹. Subsequently, a new family of quasi-1D superconductors $A_2Cr_3As_3$ ($A=K,Rb,Cs$) has been discovered at ambient pressure with T_c up to $6.1K$ ²⁻⁴. The key building block of $A_2Cr_3As_3$ is the 1D $[(Cr_3As_3)^{2-}]_\infty$ double-walled subnanotubes (Fig. 1), which are separated by columns of K^+ ions, in contrast to the layered iron-pnictide and copper-oxide high T_c superconductors.

This new family exhibits interesting properties in both the normal and SC states. In the normal state, the resistivity follows $\rho(T) = \rho_0 + AT$ in a wide temperature region, different from the usual Fermi liquid behavior $\rho_0 + AT^{2-4}$. NMR measurements on $K_2Cr_3As_3$ showed a power-law temperature dependence $1/T_1 \sim T^{0.75}$ above T_c , which is neither $1/T_1 \sim T$ for a Fermi liquid nor Curie-Weiss behavior $1/T_1 T \sim C/(T + \theta)$ for an AFM⁵. Below T_c , the electronic contribution to the specific heat $C_e(T)$ deviates from the BCS scenario, and the extrapolated upper critical field H_{c2} exceeds the Pauli limit²⁻⁴. The Hebel-Slichter coherence peak of $1/T_1$ is absent in $K_2Cr_3As_3$ NMR measurement⁵. London penetration

depth measurement for $K_2Cr_3As_3$ shows linear temperature dependence, $\Delta\lambda(T) \sim T$, at temperatures $T \ll T_c$ ⁶. All these experiments are very difficult to explain within electron-phonon coupling mechanism, and suggest unconventional nature of superconductivity.

The electronic structure of $K_2Cr_3As_3$ has been investigated by Jiang *et al.*⁷ using density functional theory (DFT), which is confirmed by later calculation⁸. There are three energy bands at the Fermi level: two quasi-1D α - and β -bands with flat Fermi surfaces, and a 3D γ -band. It is natural to ask the question, which band is responsible for the superconductivity? On one hand, the linear temperature dependent resistivity and the power-law $1/T_1$ in NMR indicate a quasi-1D Tomonaga-Luttinger liquid; on the other hand, upper critical field measurement H_{c2} implies a 3D superconductor⁹. In this Letter, we shall carry out theoretical study to address this issue. We shall focus on $K_2Cr_3As_3$ and the theory may be extended to other alkali chromium arsenides.

We begin with constructing the Hamiltonian by using symmetries. The space group for $A_2Cr_3As_3$ lattices is $P\bar{6}m2$ and the corresponding point group is D_{3h} .²⁻⁴ We shall also assume that the time reversal symmetry remains unbroken, and consider a system described by the Hamiltonian

$$H = H_0 + H_{int},$$

where H_0 is the non-interacting part and H_{int} is the interacting Hamiltonian.

Tight-binding model. We assume H_0 to be given by a tight-binding Hamiltonian. For $K_2Cr_3As_3$, there are three Fermi surfaces corresponding to the α , β and γ bands. Minimally, we need three orbitals per unit cell (per Cr_6As_6 cluster). From the DFT calculation, there are three low energy molecular orbitals. Two of them belong to 2D irreducible representation E' of D_{3h} group, and the other one is in 1D representation A'_1 . We denote two E' states as $|1\rangle$ and $|2\rangle$ and the A'_1 state as $|3\rangle$. Neglecting spin-orbit coupling, the tight-binding Hamil-

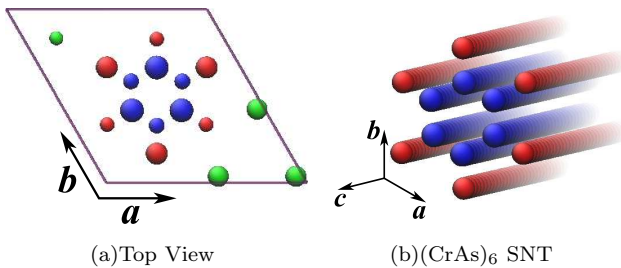


FIG. 1: Crystal structure of $A_2Cr_3As_3$. (a) Top view and (b) the $(Cr_6As_6)_\infty$ sub-nanotube. In panel (a), larger and smaller atoms are at $z=0.5$ and $z=0$, respectively. In both panels, green balls indicate alkaline atoms, red balls arsenic atoms, and blue balls chromium atoms.

tonian H_0 can be constructed from these three orbitals,

$$H_0 = \sum_{\mathbf{k}mn s} c_{\mathbf{k}ms}^\dagger \xi_{\mathbf{k}mn} c_{\mathbf{k}ns}, \quad (1)$$

where $m, n = 1, 2, 3$ are the three molecular orbitals, $s = \uparrow, \downarrow$ is the spin index, $c_{\mathbf{k}ms}^\dagger (c_{\mathbf{k}ms})$ creates an m -orbital electron with spin s . In the basis $\{|1\rangle, |2\rangle, |3\rangle\}$, $\xi_{\mathbf{k}mn}$ can be written in terms of matrix form

$$\hat{\xi}_{\mathbf{k}} = \sum_{\tau=0}^8 \xi_{\mathbf{k}}^\tau \lambda_\tau, \quad (2)$$

where λ_0 is the unit matrix and λ_{1-8} are Gell-Mann matrices.

We now use the symmetry to analyse $\xi_{\mathbf{k}}^\tau$, $\tau = 1, \dots, 8$. λ_{1-8} transfer as irreducible representations under D_{3h} symmetry operations. Namely, λ_0 and λ_8 transfer as A'_1 , λ_2 transfers as A'_2 , (λ_1, λ_3) , (λ_4, λ_6) and (λ_5, λ_7) transfer as E' respectively. H_0 should be invariant under all the D_{3h} symmetry operations, thereby belongs to representation A'_1 . Therefore, $\xi_{\mathbf{k}}^\tau$ can be determined using the Clebsch-Gordan coefficients.¹⁰ Since the ab -plane lattice constant $a = 9.98\text{\AA}$ is much larger than that along the c -axis $c = 4.23\text{\AA}$, we will only keep the hopping terms on ab -plane up to the first nearest neighbor (NN) bonds and those along c -axis up to the second NN bonds. To do this, we set the Bravais lattice basis $\mathbf{a} = (\frac{a}{2}, -\frac{\sqrt{3}a}{2}, 0)$, $\mathbf{b} = (\frac{a}{2}, \frac{\sqrt{3}a}{2}, 0)$, $\mathbf{c} = (0, 0, c)$ (see Fig.1), and introduce $k_a = \mathbf{k} \cdot \mathbf{a}$, $k_b = \mathbf{k} \cdot \mathbf{b}$, $k_c = \mathbf{k} \cdot \mathbf{c}$, and some harmonic functions on the ab plane,

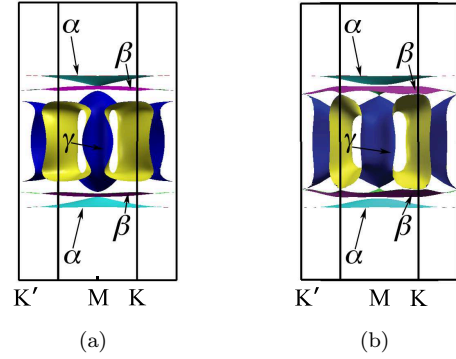
$$\begin{aligned} s_{x^2+y^2}(\mathbf{k}) &= \cos k_a + \cos k_b + \cos(k_a + k_b), \\ p_x(\mathbf{k}) &= 2 \sin(k_a + k_b) + \sin k_a + \sin k_b, \\ p_y(\mathbf{k}) &= \sqrt{3}(\sin k_b - \sin k_a), \\ d_{x^2-y^2}(\mathbf{k}) &= \cos k_a + \cos k_b - 2 \cos(k_a + k_b), \\ d_{xy}(\mathbf{k}) &= -\sqrt{3}(\cos k_b - \cos k_a). \end{aligned} \quad (3)$$

It is easy to verify that $s_{x^2+y^2} \propto 1 - \frac{1}{4}(k_x^2 + k_y^2)$, $p_x \propto k_x$, $p_y \propto k_y$, $d_{x^2-y^2} \propto k_x^2 - k_y^2$ and $d_{xy} \propto k_x k_y$ at small ka . Thus, we have $\xi_{\mathbf{k}}^2 = 0$, and other nonzero $\xi_{\mathbf{k}}^\tau$'s,

$$\begin{aligned} \xi_{\mathbf{k}}^0 &= 2t_1 \cos k_c + 2t_4 \cos 2k_c + 2t_2 s_{x^2+y^2}(\mathbf{k}), \\ \xi_{\mathbf{k}}^8 &= 2t'_1 \cos k_c + 2t'_4 \cos 2k_c + 2t'_2 s_{x^2+y^2}(\mathbf{k}), \\ \xi_{\mathbf{k}}^5 &= A p_x(\mathbf{k}), \\ \xi_{\mathbf{k}}^7 &= A p_y(\mathbf{k}), \\ \xi_{\mathbf{k}}^1 &= B d_{xy}(\mathbf{k}), \\ \xi_{\mathbf{k}}^3 &= B d_{x^2-y^2}(\mathbf{k}), \\ \xi_{\mathbf{k}}^4 &= C d_{x^2-y^2}(\mathbf{k}), \\ \xi_{\mathbf{k}}^6 &= -C d_{xy}(\mathbf{k}), \end{aligned} \quad (4)$$

where $A = (t_3 + t_5 \cos k_c)$, $B = (\tilde{t}_3 + \tilde{t}_5 \cos k_c)$, $C = (t'_3 + t'_5 \cos k_c)$. By fitting the DFT band structure of $\text{K}_2\text{Cr}_3\text{As}_3$, we obtain a set of parameters (in eV) as following: $t_1 = 0.2237$, $t_4 = -0.0566$, $t_2 = -0.0036$, $t'_1 = -0.0545$, $t'_4 = 0.0214$, $t'_2 = 0.0065$, $t_3 = 0.0240$, $t_5 = 0.0068$, $\tilde{t}_3 = -0.0114$, $\tilde{t}_5 = -0.0099$, $t'_3 = -0.0069$, $t'_5 = -0.0059$. We also obtain the chemical potential $\mu_{chem} = 0.2323$ eV. As shown in Fig. 2, the set of parameters well reproduces the Fermi surfaces. They also reproduce the energy dispersion along high symmetry lines and the density of states (DOS) near the Fermi level well.

FIG. 2: Comparison of the Fermi surfaces for $\text{K}_2\text{Cr}_3\text{As}_3$ obtained from the DFT calculation (a), and from the present model Hamiltonian (b). The α , β and γ bands are labelled. The Γ point is at the center of the Brillouin zone.



By diagonalizing H_0 we obtain three energy bands with dispersion $\epsilon_{\mathbf{k}\mu}$ and eigen-wavefunctions $\phi_{\mathbf{k}\mu}^m$, hereafter μ is the band index. The bare susceptibility tensor $\chi_0(\mathbf{q})$ is defined as

$$\begin{aligned} \chi_0^{mn, m' n'}(\mathbf{q}) &= -\frac{1}{N} \sum_{\mathbf{k}} \sum_{\mu\nu} \frac{\phi_{\mathbf{k}\mu}^m \phi_{\mathbf{k}\mu}^{m'*} \phi_{\mathbf{k}+\mathbf{q}\nu}^{n'} \phi_{\mathbf{k}+\mathbf{q}\nu}^{n*}}{\epsilon_{\mathbf{k}\mu} - \epsilon_{\mathbf{k}+\mathbf{q}\nu}} \\ &\times [f(\epsilon_{\mathbf{k}\mu}) - f(\epsilon_{\mathbf{k}+\mathbf{q}\nu})], \end{aligned} \quad (5)$$

where $f(\epsilon_{\mathbf{k}\mu})$ is the Fermion occupation number, N is the number of unit cells. Note that $\chi_0(\mathbf{q})$ can be also written as a 9×9 matrix in the two-body orbital space spanned by the basis $\{|m\rangle \otimes |n\rangle : m, n = 1, 2, 3\}$.

Interaction: Now we consider the electron-electron interaction. In the spirit of Hubbard approximation, i.e. retaining only the intra-unit-cell terms, we obtain the interacting Hamiltonian which respects D_{3h} symmetry (see Appendix A for details),

$$\begin{aligned}
H_{int} = & \frac{1}{2} \sum_i \left\{ \sum_{m=1}^2 \sum_{\sigma} [U_1 c_{im\sigma}^\dagger c_{im\bar{\sigma}}^\dagger c_{im\bar{\sigma}} c_{im\sigma} + J c_{im\sigma}^\dagger c_{im\bar{\sigma}}^\dagger c_{im\bar{\sigma}} c_{im\sigma} + J' (c_{im\sigma}^\dagger c_{im\bar{\sigma}}^\dagger c_{i3\bar{\sigma}} c_{i3\sigma} + h.c.)] \right. \\
& + \sum_{m=1}^2 \sum_{\sigma\sigma'} (U_2 c_{im\sigma}^\dagger c_{im\sigma'}^\dagger c_{im\sigma'} c_{im\sigma} + J c_{im\sigma}^\dagger c_{im\sigma'}^\dagger c_{im\sigma'} c_{im\sigma} + U_2' c_{im\sigma}^\dagger c_{i3\sigma'}^\dagger c_{i3\sigma'} c_{im\sigma} + J' c_{im\sigma}^\dagger c_{i3\sigma'}^\dagger c_{im\sigma'} c_{i3\sigma}) \\
& \left. + \sum_{\sigma} U_1' c_{i3\sigma}^\dagger c_{i3\bar{\sigma}}^\dagger c_{i3\bar{\sigma}} c_{i3\sigma} \right\}, \tag{6}
\end{aligned}$$

where \bar{m} is the opposite orbital to m within E' representation ($\bar{1} = 2$ and $\bar{2} = 1$), and $\bar{\sigma}$ is the opposite spin to σ . Here U_1 , U_2 and J are intra-orbital repulsion, inter-orbital repulsion and Hund's coupling for the two E' states, which satisfy that $U_1 = U_2 + 2J$. U_1' is the intra-orbital repulsion for the A_1' state, and J' involves one of E' states and the A_1' state.

By Fourier transformation, we have

$$\begin{aligned}
H_{int} = & \frac{1}{2} \sum_{\mathbf{k}\mathbf{k}'\mathbf{q}} \sum_{mnm'n'} \Gamma_0^{mn,m'n'}(\mathbf{k}, \mathbf{k} - \mathbf{q}; \mathbf{k}', \mathbf{k}' + \mathbf{q}) \\
& \times c_{\mathbf{k}m\sigma}^\dagger c_{\mathbf{k}'m'\sigma'}^\dagger c_{\mathbf{k}'+\mathbf{q}n'\sigma'} c_{\mathbf{k}-\mathbf{q}n\sigma}, \tag{7}
\end{aligned}$$

where the bare vertex function $\Gamma_0^{mn,m'n'}(\mathbf{k}, \mathbf{k} - \mathbf{q}; \mathbf{k}', \mathbf{k}' + \mathbf{q})$ can be written as a matrix in the two-body orbital space,

$$\hat{\Gamma}_0(\mathbf{k}, \mathbf{k} - \mathbf{q}; \mathbf{k}', \mathbf{k}' + \mathbf{q}) = (1 - \delta_{\sigma\sigma'}) \hat{\Gamma}_s + \delta_{\sigma\sigma'} \hat{\Gamma}_t, \tag{8}$$

where $\hat{\Gamma}_t$ is bare vertex in the equal-spin channel and $\hat{\Gamma}_s$ is in the opposite-spin channel. The two-body orbital space can be decomposed to subspaces $\{|11\rangle, |22\rangle, |33\rangle\} \oplus \{|12\rangle, |21\rangle\} \oplus \{|13\rangle, |13\rangle\} \oplus \{|23\rangle, |32\rangle\}$. Thus, $\hat{\Gamma}_s$ and $\hat{\Gamma}_t$ are block diagonal in this set of basis,

$$\hat{\Gamma}_s = \begin{pmatrix} U_1 & U_2 & U_2' \\ U_2 & U_1 & U_2' \\ U_2' & U_2' & U_1' \end{pmatrix} \oplus J\Pi \oplus J'\Pi \oplus J'\Pi, \tag{9a}$$

$$\hat{\Gamma}_t = \begin{pmatrix} 0 & U_2 & U_2' \\ U_2 & 0 & U_2' \\ U_2' & U_2' & 0 \end{pmatrix} \oplus J\sigma_1 \oplus J'\sigma_1 \oplus J'\sigma_1, \tag{9b}$$

where σ_1 is Pauli matrix and $\Pi = 1 + \sigma_1$ is a 2×2 matrix.

Effective pairing interaction. For weak coupling, the full vertex function $\Gamma_{\sigma\sigma'}^{mn,m'n'}(\mathbf{k}, \mathbf{k} - \mathbf{q}; \mathbf{k}', \mathbf{k}' + \mathbf{q})$ can be evaluated diagrammatically, for instance, through the random phase approximation (RPA). To study the SC pairing, we only need to keep the vertices in pairing channels with $\mathbf{k}' = -\mathbf{k}$, say, $\hat{\Gamma}_{\sigma\sigma'}(\mathbf{k}, \mathbf{k}'; -\mathbf{k}, -\mathbf{k}') \equiv \hat{V}_{\sigma\sigma'}(\mathbf{k}, \mathbf{k}')$. Therefore, $\hat{V}_{\sigma\sigma'}(\mathbf{k}, \mathbf{k}') = (1 - \delta_{\sigma\sigma'}) \hat{V}_s(\mathbf{k}, \mathbf{k}') + \delta_{\sigma\sigma'} \hat{V}_t(\mathbf{k}, \mathbf{k}')$ serves as an effective pairing interaction to study superconductivity instability.

In study of the cuprates, Scalapino et al. used RPA to calculate $\hat{V}_{\sigma\sigma'}(\mathbf{k}, \mathbf{k}')$ in a single Hubbard model.¹¹ The

RPA involves two types of Feynman diagrams in addition to the bare vertex function $\hat{V}_0(\mathbf{k}, \mathbf{k}')$ (see Appendix C for details). One contains the bubble diagrams, and the other contains the ladder diagrams with Cooperon. Here we generalize the calculation in Ref.¹¹ to the multi-orbital case. The effective pairing interaction $\hat{V}_{s(t)}(\mathbf{k}, \mathbf{k}')$ from the bubble diagrams is

$$\begin{aligned}
\hat{V}_{s(t)}^{bub}(\mathbf{k}, \mathbf{k}') = & \frac{1}{2} \left\{ (\hat{\Gamma}_t + \hat{\Gamma}_s) [1 + \hat{\chi}_0(\mathbf{q})(\hat{\Gamma}_t + \hat{\Gamma}_s)]^{-1} \right. \\
& \left. \mp (\hat{\Gamma}_t - \hat{\Gamma}_s) [1 + \hat{\chi}_0(\mathbf{q})(\hat{\Gamma}_t - \hat{\Gamma}_s)]^{-1} \right\} \tag{10}
\end{aligned}$$

where \mp takes $-$ for s and $+$ for t . The effective pairing from the ladder diagrams is

$$\hat{V}_{s(t)}^{lad}(\mathbf{k}, \mathbf{k}') = \tilde{\Gamma}_{s(t)} \hat{\chi}_0(\mathbf{p}) \tilde{\Gamma}_{s(t)} [1 - \hat{\chi}_0(\mathbf{p}) \tilde{\Gamma}_{s(t)}]^{-1}, \tag{11}$$

where $\mathbf{p} = \mathbf{k} + \mathbf{k}'$ and $\mathbf{q} = \mathbf{k} - \mathbf{k}'$ (See Appendix C for details). For the notation, matrix \hat{A} is related to matrix \tilde{A} via the following relation,

$$\tilde{A}_{mn,m'n'} = \hat{A}_{nn',m'm}.$$

We can also project effective pairing potential $\hat{V}_{\sigma\sigma'}(\mathbf{k}, \mathbf{k}')$ into three single particle bands through

$$V_{\sigma\sigma'}^{\mu\nu}(\mathbf{k}, \mathbf{k}') = \sum_{mnm'n'} \phi_{\mathbf{k}\mu}^{m*} \phi_{-\mathbf{k}\mu}^{m'*} V_{\sigma\sigma'}^{mn,m'n'}(\mathbf{k}, \mathbf{k}') \phi_{\mathbf{k}'\nu}^n \phi_{-\mathbf{k}'\nu}^{n'}, \tag{12}$$

where $\phi_{\mathbf{k}\mu}^m$ is the single particle eigenwavefunction in the μ -band.

Superconducting pairing instability. Because the three Fermi surfaces have different shapes, \mathbf{k} and $-\mathbf{k}$ are always in the same band for \mathbf{k} near the Fermi surfaces. For weak coupling, we only consider intra-band pairing (\mathbf{k} to $-\mathbf{k}$). A single band gap function can be written as

$$\Delta(\mathbf{k}) = i [\sigma_0 \psi(\mathbf{k}) + \sigma \cdot \mathbf{d}(\mathbf{k})] \sigma_2, \tag{13}$$

where $\psi(\mathbf{k}) = \psi(-\mathbf{k})$ is the spin-singlet gap function, and the d -vector $\mathbf{d}(\mathbf{k}) = -\mathbf{d}(-\mathbf{k})$ describes the spin-triplet pairing, σ_0 is the unit matrix, $\sigma_{1,2,3}$ are Pauli matrices. To measure the intra-band SC pairing instability, we follow Scalapino *et al.*,¹¹ and introduce a dimensionless coupling constant

$$\Lambda_\mu = - \frac{\int \frac{dS_{\mathbf{k}\mu}}{|\mathbf{v}_{\mathbf{k}\mu}|} \int \frac{dS_{\mathbf{k}'\mu}}{|\mathbf{v}_{\mathbf{k}'\mu}|} \sum_{\sigma\sigma'} g_{\sigma\sigma'}^\mu(\mathbf{k})^* V_{\sigma\sigma'}^{\mu\mu}(\mathbf{k}, \mathbf{k}') g_{\sigma\sigma'}^\mu(\mathbf{k}')}{(2\pi)^3 \int \frac{dS_{\mathbf{k}\mu}}{|\mathbf{v}_{\mathbf{k}\mu}|} \sum_{\sigma\sigma'} |g_{\sigma\sigma'}^\mu(\mathbf{k})|^2},$$

where $\int dS_{\mathbf{k}\mu}$ is the integration over the μ -band Fermi surface and $\mathbf{v}_{\mathbf{k}\mu}$ is the Fermi velocity, the μ -band form factor $g_{\sigma\sigma'}^{\mu}(\mathbf{k}) \propto \Delta_{\sigma\sigma'}(\mathbf{k})$.

In the absence of the spin-orbit coupling, the spin-singlet component $\psi(\mathbf{k})$ will not mix with the spin-triplet component $\mathbf{d}(\mathbf{k})$ in Eq.(13). The possible single-band SC gap functions on hexagonal lattice are listed in Table I up to the first and second NN bonds¹².

TABLE I: Superconducting gap functions $\psi(\mathbf{k})$ and $\mathbf{d}(\mathbf{k})$ on hexagonal lattice. The gap functions are intra-band and are classified according to D_{3h} group irreducible representation Γ . The functions $s_{x^2+y^2}$, p_x , p_y , $d_{x^2-y^2}$, and d_{xy} have been defined in Eq.(3). Other functions are defined as follows, $p_z = \sin k_c$, $d_{z^2} = \cos k_c$, $f_{x(x^2-3y^2)} = \sin k_a + \sin k_b - \sin(k_a + k_b)$, $f_{y(3x^2-y^2)} = \sin(2k_a + k_b) - \sin(k_a + 2k_b) - \sin(k_a - k_b)$.

Γ	spin-singlet $\psi(\mathbf{k})$	spin-triplet $\mathbf{d}(\mathbf{k})$
A'_1	$1, s_{x^2+y^2}, d_{z^2}$	$f_{y(3x^2-y^2)}\hat{z}$
A'_2		$f_{x(x^2-3y^2)}\hat{z}$
E'	$(d_{x^2-y^2}, d_{xy})$	$(p_x, p_y)\hat{z}, p_z(\hat{x}, \hat{y})$
A''_1	$p_z f_{y(3x^2-y^2)}$	$p_x\hat{x} + p_y\hat{y}, p_z\hat{z}$
A''_2	$p_z f_{x(x^2-3y^2)}$	$p_y\hat{x} - p_x\hat{y}$
E''	$p_z(p_x, p_y)$	$(p_x\hat{x} - p_y\hat{y}, p_y\hat{x} + p_x\hat{y})$

We next examine all the pairing states in Table I to investigate which pairing channel will dominate. For simplicity, we set $U_1 = U'_1 = U$, $U'_2 = U_2$ and $J' = J$ at first. The relevant Λ_{μ} 's are plotted as functions of J/U in Fig. 3, and those Λ_{μ} not plotted have either negative or negligibly small values.

Fig. 3(a) shows the pair coupling constant in various channels for $U = 0.5$ eV. Results for $U < 0.5$ eV are similar. The spin-triplet $f_{y(3x^2-y^2)}$ state in the γ -band appears at a finite J/U and become dominant when $J/U > 1/3$. The $f_{y(3x^2-y^2)}$ state has a line nodal gap. Fig. 3(c) plots the results at $U = 2$ eV, to represent large U . In that case, the spin-triplet $p_z\hat{z}$ state at the α -band dominates in all the realistic region of $J/U < 0.45$. The $p_z\hat{z}$ state has a full gap at the quasi-1D α -band Fermi surface. In the intermediate region, e.g., $U = 1.0$ eV, $p_z\hat{z}$ and $f_{y(3x^2-y^2)}$ state compete against each other, $p_z\hat{z}$ dominates at small J/U , while $f_{y(3x^2-y^2)}$ state become strong at large J/U . We have also calculated the pair coupling constant for $J' \neq J$ while keeping $U_1 = U'_1 = U$ and $U'_2 = U_2$. The results are similar in a wide parameter region $0.5 < J'/J < 2.0$. Note that at large U and J/U , the SC pairing is found in the β -band with pairing symmetry $p_x\hat{x} \pm p_y\hat{y}$ and $p_y\hat{x} \pm p_x\hat{y}$, which gives point nodal in the gap function. However, Λ_{μ} for these point nodally gapped states are tiny.

Note that the deviation of our tight-binding model from DFT results in some details should not change the above statements qualitatively. Because it is the Fermi surface shape and DOS near the Fermi level that determine Λ_{μ} and pairing symmetry in weak coupling.

Discussions and Summary We would like to mention some issues which have not been addressed in this paper

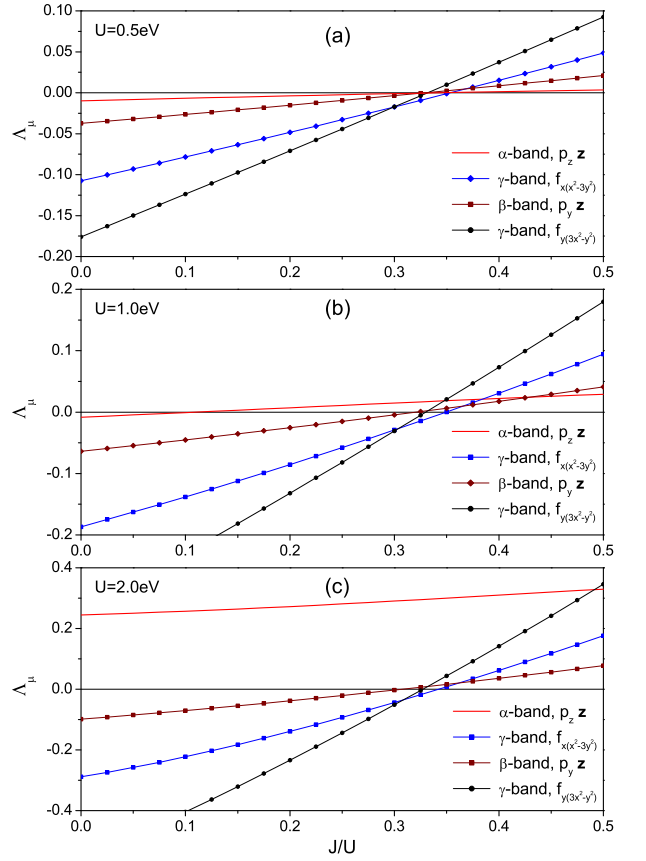


FIG. 3: The dimensionless pair coupling constant Λ_{μ} vs J/U for (a) $U = 0.5$ eV, (b) $U = 1.0$ eV and (c) $U = 2.0$ eV. Here we have set $U_1 = U'_1 = U$, $U'_2 = U_2$ and $J' = J$. All the dominated states are spin-triplet pairing states. (a) $U = 0.5$ eV, $f_{y(3x^2-y^2)}$ appear and dominate when $J/U > 1/3$. (b) $U = 1.0$ eV, $p_z\hat{z}$ state and $f_{y(3x^2-y^2)}$ compete against each other. (c) $U = 2.0$ eV, $p_z\hat{z}$ state dominates over most J/U .

but may be interesting for future work. (i) We neglect spin-orbit coupling in the theory for simplicity. Actually the D_{3h} lattice breaks inversion symmetry, and the spin-orbit coupling may mix spin singlet and triplet states within the same D_{3h} irreducible representation in Table I. (ii) Since molecular orbitals are more extended than atomic orbitals, U and J are estimated to be smaller than or comparable to the bandwidth. In this paper we start with weak coupling to study SC instability. However, $A_2\text{Cr}_3\text{As}_3$ lattice is quasi-1D, an alternative approach would be to model the system as a coupled Tomonaga-Luttinger liquid. (iii) Although we only consider the intra-band pairing states in this paper, the inter-band pair scatterings of Cooper pairs are included in the RPA calculation, since the multi-orbital susceptibility tensor is used and both particle-hole channels (bubble diagrams) and particle-particle channels (ladder diagrams) are included in the RPA.

We would like to make comments on the on-site approximation in the Hubbard model too. Although the three molecular orbitals are more extended in compari-

son with the atomic orbitals, these molecular orbitals are quite localized. The inter-unit-cell electron interaction is a small fraction of the intra-unit-cell (see Appendix B). Therefore the inter-cell interaction should play a less important role in our analysis.

The spin-triplet pairing states in our study originates from the Hund's coupling. The Hund's coupling favors spin-triplet states of two different molecular orbitals on the same molecule, and Cooper pairs can be formed in the spin-triplet channel. That's the reason why the triplet pairing channels get instability when the Hund's coupling J is larger than the inter-orbital repulsion U_2 in the weak coupling scenario¹³. Moreover, the DOS at Fermi level at the 3D γ -band is much larger than those at two quasi-1D bands (3 to 5 times), it is expected that the superconducting instability will dominate at the 3D γ -band at small U .

In summary, we have proposed a minimal model to study superconductivity in $A_2Cr_3As_3$ ($A=K,Rb,Cs$), which involves three molecular orbital states in each unit cell. With the help of symmetry, we have deduced a tight-binding model with 3 molecular orbitals for the system, which compares well with the results of the density functional theory. We have derived effective pairing interactions within the RPA, and found that the dominant pairing channel is always spin-triplet. For small U , a spin-triplet state with line nodal gap, $f_{y(3x^2-y^2)}$, at the 3D γ -band will dominate at moderate Hund's coupling. While for large U , a spin-triplet fully gapped state, $p_z\hat{z}$, will dominate at the quasi-1D α -band. The state we find at small U appears to be most relevant to the compound. The pairing state of $f_{y(3x^2-y^2)}$ has nodal lines on planes $k_a = k_b$, $k_a = -2k_b$ and $k_b = -2k_a$, say, Γ - K - L - A planes on hexagonal lattices. The Γ - K - L - A planes cross small sections at γ -Fermi surface. Our theory at small U predicts line zeroes in gap function and appears to be consistent with existing experiments showing non-BCS gap function and particularly the low temperature London penetration depth measurement. Our prediction can be tested in further experiments including angle resolved photoemission spectroscopy.

Acknowledgment We would like to thank G.H. Cao, Z.A. Xu, H.Q. Yuan, F.L. Ning, J. Zhao and H. Yao and D. F. Agterberg for helpful discussions. This work is supported in part by National Key R&D Program of China (No.2016YFA0300202), National Basic Research Program of China (No.2014CB921201/2014CB921203), NSFC (No.11374256/11274269/11274006), NSF of Zhejiang Province (No. LR12A04003).

Appendix A: Derive the interacting part for three-orbital Hubbard model

The electron field operator $\hat{\psi}_\sigma(\vec{r})$ can be expanded in terms of a complete set of Wannier functions,

$$\hat{\psi}_\sigma(\vec{r}) = \sum_m \sum_i w_{im}(\vec{r})c_{im\sigma}, \quad (A1)$$

where $c_{im\sigma}$ annihilates an electron with orbital m and spin σ at lattice site i . A generic interacting Hamiltonian is given by

$$H_{int} = \frac{1}{2} \sum_{\sigma\sigma'} \int \hat{\psi}_\sigma^\dagger(\vec{r}_1)\hat{\psi}_{\sigma'}^\dagger(\vec{r}_2)V(\vec{r}_1 - \vec{r}_2) \times \hat{\psi}_{\sigma'}(\vec{r}_2)\hat{\psi}_\sigma(\vec{r}_1)d\vec{r}_1d\vec{r}_2, \quad (A2)$$

where $V_{ext}(\vec{r})$ is external periodic potential, and $V(\vec{r}_1 - \vec{r}_2)$ is the screened Coulomb interaction. H_0 can be written as a tight-binding model and we shall focus on the interacting part H_{int} . In the spirit of a Hubbard type approximation, i.e. retaining only the terms on the same lattice site, we have

$$H_{int} = \frac{1}{2} \sum_i \sum_{mm'n'} \sum_{\sigma\sigma'} V_{mm',n'n} \times c_{im\sigma}^\dagger c_{im'\sigma'}^\dagger c_{in'\sigma'} c_{in\sigma}, \quad (A3)$$

where

$$V_{mm',n'n} = \int w_{im}^*(\vec{r}_1)w_{im'}^*(\vec{r}_2)V(\vec{r}_1 - \vec{r}_2) \times w_{in'}(\vec{r}_2)w_{in}(\vec{r}_1)d\vec{r}_1d\vec{r}_2. \quad (A4)$$

Let's consider nonvanishing $V_{mm',n'n}$ according to D_{3h} group symmetry. Since the interaction $V(\vec{r}_1 - \vec{r}_2) = V(|\vec{r}_1 - \vec{r}_2|)$ respects the full point group symmetry and belong to the A_1 representation. Whether a $V_{mm',n'n}$ vanishes can be determined by the Clebsch-Gordan coefficients of D_{3h} group.

Firstly, for $m, n = 1, 2$, the nonzero $V_{mm',n'n}$ can be written in terms of the integrals explicitly,

$$\begin{aligned} V_{mm,mm} &= \int |w_{im}(\vec{r}_1)|^2 V(\vec{r}_1 - \vec{r}_2) |w_{im}(\vec{r}_2)|^2 d\vec{r}_1 d\vec{r}_2 \\ &= U_1, \\ V_{m\bar{m},\bar{m}m} &= \int |w_{im}(\vec{r}_1)|^2 V(\vec{r}_1 - \vec{r}_2) |w_{i\bar{m}}(\vec{r}_2)|^2 d\vec{r}_1 d\vec{r}_2 \\ &= U_2, \\ V_{m\bar{m},m\bar{m}} &= \int w_{im}^*(\vec{r}_1)w_{i\bar{m}}(\vec{r}_1)V(\vec{r}_1 - \vec{r}_2) \\ &\quad \times w_{i\bar{m}}^*(\vec{r}_2)w_{im}(\vec{r}_2)d\vec{r}_1 d\vec{r}_2 = J, \\ V_{mm,\bar{m}\bar{m}} &= \int w_{im}^*(\vec{r}_1)w_{i\bar{m}}(\vec{r}_1)V(\vec{r}_1 - \vec{r}_2) \\ &\quad \times w_{i\bar{m}}(\vec{r}_2)w_{im}^*(\vec{r}_2)d\vec{r}_1 d\vec{r}_2 = J^*. \end{aligned}$$

where U_1 is the intra-orbital interaction and U_2 is the inter-orbital interaction. If one chooses the Wannier function to be real, then $J^* = J$, and J is the Hund's exchange energy.

Secondly, we can choose that $|1\rangle$ transfers as x and $|2\rangle$ transfers as y under D_{3h} symmetry operations. Note that $V(\vec{r}_1 - \vec{r}_2)$ is invariant not only under D_{3h} symmetry operations, but also under all the $O(3)$ symmetry operations. So that $V_{xx,xx} = V_{yy,yy} = U_1$. Under a C_3 rotation

along the c -axis, the two Wannier functions $|1\rangle$ and $|2\rangle$ (denoted by x and y) transfer as

$$\begin{aligned} w_x &\rightarrow \cos\theta w_x + \sin\theta w_y, \\ w_y &\rightarrow -\sin\theta w_x + \cos\theta w_y, \end{aligned}$$

where $\theta = \frac{2\pi}{3}$. The integral $V_{xx,xx}$ should keep invariant under this operation. Assuming w_x and w_y are real, after straightforward algebra, we have

$$\begin{aligned} U_1 &= (\cos^4\theta + \sin^4\theta)U_1 + 2U_2 \cos^2\theta \sin^2\theta \\ &\quad + 4\cos^2\theta \sin^2\theta J, \end{aligned}$$

where the transformation properties under C_2 are used. From the above, we have

$$U_1 = U_2 + 2J.$$

Thirdly, we involve the state $|3\rangle$. For $m, m' = 1, 2$ (or x, y), the relevant nonvanishing terms are given in the following,

$$\begin{aligned} V_{33,33} &= \int |w_{i3}(\vec{r}_1)|^2 V(\vec{r}_1 - \vec{r}_2) |w_{i3}(\vec{r}_2)|^2 d\vec{r}_1 d\vec{r}_2 \\ &= U'_1, \\ V_{3m,m3} &= \int |w_{im}(\vec{r}_1)|^2 V(\vec{r}_1 - \vec{r}_2) |w_{i3}(\vec{r}_2)|^2 d\vec{r}_1 d\vec{r}_2 \\ &= U'_2, \\ V_{m3,m3} &= \int w_{im}^*(\vec{r}_1) w_{i3}(\vec{r}_1) V(\vec{r}_1 - \vec{r}_2) \\ &\quad \times w_{i3}^*(\vec{r}_2) w_{im}(\vec{r}_2) d\vec{r}_1 d\vec{r}_2 = J', \\ V_{mm',33} &= \int w_{im}^*(\vec{r}_1) w_{i3}(\vec{r}_1) V(\vec{r}_1 - \vec{r}_2) \\ &\quad \times w_{im'}^*(\vec{r}_2) w_{i3}(\vec{r}_2) d\vec{r}_1 d\vec{r}_2 = J''_{mm'}. \end{aligned}$$

When Wannier functions are real, $J''_{mm'} = J'$. For $m \neq m'$, we set $m = x$ and $m' = y$, thus under the C_3 rotation,

$$\begin{aligned} J''_{xx} &= \cos^2\theta J''_{xx} + \sin^2\theta J''_{yy} + 2\cos\theta \sin\theta J''_{xy} \\ &= J''_{xx} + 2\cos\theta \sin\theta J''_{xy}. \end{aligned}$$

The above gives rise to

$$J''_{xy} = 0.$$

Thus, we obtain H_{int} in Eq. (6) in the main text.

Appendix B: Wannier functions from density functional theory

To estimate the order of magnitude of intra-unit-cell U and inter-unit-cell interaction V , we extract the Wannier functions for the three energy bands crossing Fermi levels from the DFT calculation. It should be noted these three Wannier functions $\tilde{w}_{im=1,2,3}$ are not the molecular orbitals $w_{im=1,2,3}$ used in our tight-binding model. Indeed \tilde{w}_{im} are some linear combinations of w_{im} . So that we can

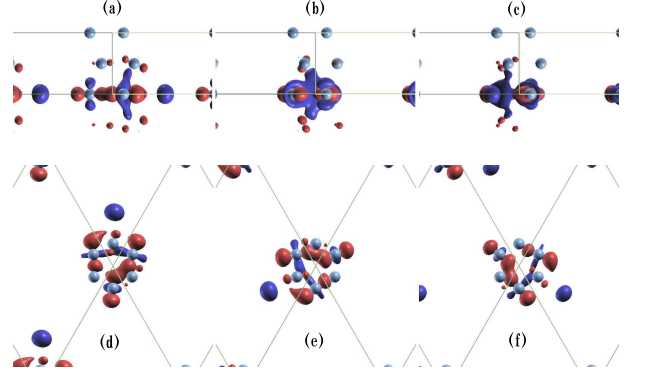


FIG. 4: Three Wannier functions from DFT calculation. (a)(b)(c) Side view of three Wannier functions. (d)(e)(f) Top view of three Wannier functions.

not calculate U_1, U_2, U'_1, U'_2 and J, J' from the Wannier functions \tilde{w}_{im} directly. However, we can roughly estimate the order of magnitude of U and V from \tilde{w}_{im} . To do this, we use unscreened Coloumb interaction e^2/r to estimate the on-site and nearest-neighboring interaction U and V ,

$$\begin{aligned} U_{mm'} &= \int |\tilde{w}_{im}(\vec{r}_1)|^2 \frac{e^2}{|\vec{r}_1 - \vec{r}_1|} |\tilde{w}_{im'}(\vec{r}_2)|^2 d\vec{r}_1 d\vec{r}_2, \\ V_{mm'} &= \int |\tilde{w}_{im}(\vec{r}_1)|^2 \frac{e^2}{|\vec{r}_1 - \vec{r}_1|} |\tilde{w}_{i+\hat{z},m'}(\vec{r}_2)|^2 d\vec{r}_1 d\vec{r}_2, \end{aligned}$$

where $i + \hat{z}$ denote the neighboring unit cell to the unit cell i along the c -axis.

It should be noted that the real interaction should be smaller due to screening effect. As mentioned, $U_{mm'}$ and $V_{mm'}$ will be reduced due to screening effect. The present values are used to estimate order of magnitude and the ratio V/U only.

TABLE II: $U_{mm'}$ and $V_{mm'}$, which should be reduced due to screening.

m	m'	$U_{mm'}(\text{eV})$	$V_{mm'}(\text{eV})$
1	1	2.195	0.169
2	2	2.128	0.161
3	3	2.143	0.155
1	2	2.082	0.163
2	3	2.068	0.154
1	3	2.107	0.159

We can also estimate the spreading of Wannier functions along the c -axis and ab -plane respectively, which

are defined by

$$r_{\parallel m}^2 = \int z^2 |\tilde{w}_{im}(\vec{r})|^2 d\vec{r},$$

$$r_{\perp m}^2 = \int (x^2 + y^2) |\tilde{w}_{im}(\vec{r})|^2 d\vec{r}.$$

It is estimated that $r_{\parallel} = 1.7 \text{ \AA}$ and $r_{\perp} = 4.8 \text{ \AA}$. For the Cr atom, the $3d$ wavefunction spreading is about $r_0 = 1.6 \text{ \AA}$. The atomic on-site interaction U for Cr is about 2 eV. Then we can estimate the interaction U for a Cr_6As_6 cluster as less than 1 eV.

Appendix C: RPA for effective pairing interaction

We shall generalized the calculation by Scalapino et al. to the multi-orbital case. Diagrammatically, RPA contains two types Feynman diagrams beside the bare vertex function $V_0(\mathbf{k}, \mathbf{k}')$ as shown in Fig. 5. One contains the bubble diagrams, the other contains the ladder diagrams with Cooperon.

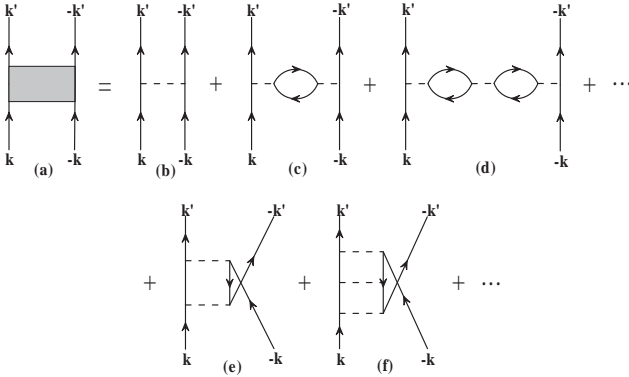


FIG. 5: Feynman diagram for RPA calculation of effective pairing interaction $V(\mathbf{k}, \mathbf{k}')$. (a) Effective vertex function $V(\mathbf{k}, \mathbf{k}')$. (b) Bare vertex function $V_0(\mathbf{k}, \mathbf{k}')$. (c) and (d) Bubble diagrams. (e) and (f) Ladder diagrams with Cooperon.

For the single orbital case, the RPA effective pairing interaction for spin-singlet and spin-triplet channels are

$$V_s(\mathbf{k}, \mathbf{k}') = \frac{U}{1 - U^2 \chi_0^2(\mathbf{k} - \mathbf{k}')} + \frac{U^2 \chi_0(\mathbf{k} + \mathbf{k}')}{1 - U \chi_0(\mathbf{k} + \mathbf{k}')},$$

$$V_t(\mathbf{k}, \mathbf{k}') = -\frac{U^2 \chi_0(\mathbf{k} - \mathbf{k}')}{1 - U^2 \chi_0^2(\mathbf{k} - \mathbf{k}')}.$$

Note that Fig. 5(c) is absent in U_s and Fig. 5(b), (d), (e) and (f) are absent in V_t because $\sigma' = \bar{\sigma}$ in the U term.

For multi-orbital case, we shall replace the numbers U and χ_0 by the bare vertex functions $\hat{\Gamma}_{s(t)}$ in Eq. (9) and susceptibility tensor $\hat{\chi}_0$ in Eq. (5) in the main text. The effective pairing interaction $\hat{V}_{s(t)}(\mathbf{k}, \mathbf{k}')$ from the bubble

diagrams are

$$\begin{aligned} \hat{V}_s^{bub}(\mathbf{k}, \mathbf{k}') &= \hat{\Gamma}_s - \hat{\Gamma}_s \hat{\chi}_0(\mathbf{q}) \hat{\Gamma}_t - \hat{\Gamma}_t \hat{\chi}_0(\mathbf{q}) \hat{\Gamma}_s \\ &\quad + \hat{\Gamma}_s \hat{\chi}_0(\mathbf{q}) \hat{\Gamma}_t \hat{\chi}_0(\mathbf{q}) \hat{\Gamma}_t \\ &\quad + \hat{\Gamma}_t \hat{\chi}_0(\mathbf{q}) \hat{\Gamma}_s \hat{\chi}_0(\mathbf{q}) \hat{\Gamma}_t \\ &\quad + \hat{\Gamma}_t \hat{\chi}_0(\mathbf{q}) \hat{\Gamma}_t \hat{\chi}_0(\mathbf{q}) \hat{\Gamma}_s \\ &\quad + \hat{\Gamma}_s \hat{\chi}_0(\mathbf{q}) \hat{\Gamma}_s \hat{\chi}_0(\mathbf{q}) \hat{\Gamma}_s + \dots \\ &\quad + \hat{\Gamma}_s \hat{\chi}_0(\mathbf{p}) \hat{\Gamma}_s + \hat{\Gamma}_s \hat{\chi}_0(\mathbf{p}) \hat{\Gamma}_s \hat{\chi}_0(\mathbf{p}) \hat{\Gamma}_s + \dots \\ &= \frac{1}{2} (\hat{\Gamma}_t + \hat{\Gamma}_s) [1 + \hat{\chi}_0(\mathbf{q}) (\hat{\Gamma}_t + \hat{\Gamma}_s)]^{-1} \\ &\quad - \frac{1}{2} (\hat{\Gamma}_t - \hat{\Gamma}_s) [1 + \hat{\chi}_0(\mathbf{q}) (\hat{\Gamma}_t - \hat{\Gamma}_s)]^{-1} \end{aligned}$$

and

$$\begin{aligned} \hat{V}_t^{bub}(\mathbf{k}, \mathbf{k}') &= \hat{\Gamma}_t - \hat{\Gamma}_s \hat{\chi}_0(\mathbf{q}) \hat{\Gamma}_s - \hat{\Gamma}_t \hat{\chi}_0(\mathbf{q}) \hat{\Gamma}_t \\ &\quad + \hat{\Gamma}_t \hat{\chi}_0(\mathbf{q}) \hat{\Gamma}_t \hat{\chi}_0(\mathbf{q}) \hat{\Gamma}_t \\ &\quad + \hat{\Gamma}_t \hat{\chi}_0(\mathbf{q}) \hat{\Gamma}_s \hat{\chi}_0(\mathbf{q}) \hat{\Gamma}_s \\ &\quad + \hat{\Gamma}_s \hat{\chi}_0(\mathbf{q}) \hat{\Gamma}_t \hat{\chi}_0(\mathbf{q}) \hat{\Gamma}_s \\ &\quad + \hat{\Gamma}_s \hat{\chi}_0(\mathbf{q}) \hat{\Gamma}_s \hat{\chi}_0(\mathbf{q}) \hat{\Gamma}_t + \dots \\ &\quad + \hat{\Gamma}_t \hat{\chi}_0(\mathbf{p}) \hat{\Gamma}_t + \hat{\Gamma}_t \hat{\chi}_0(\mathbf{p}) \hat{\Gamma}_t \hat{\chi}_0(\mathbf{p}) \hat{\Gamma}_t + \dots \\ &= \frac{1}{2} (\hat{\Gamma}_t + \hat{\Gamma}_s) [1 + \hat{\chi}_0(\mathbf{q}) (\hat{\Gamma}_t + \hat{\Gamma}_s)]^{-1} \\ &\quad + \frac{1}{2} (\hat{\Gamma}_t - \hat{\Gamma}_s) [1 + \hat{\chi}_0(\mathbf{q}) (\hat{\Gamma}_t - \hat{\Gamma}_s)]^{-1}, \end{aligned}$$

while those from ladder diagrams are

$$\begin{aligned} \tilde{V}_s^{lad}(\mathbf{k}, \mathbf{k}') &= \tilde{\Gamma}_s \hat{\chi}_0(\mathbf{p}) \tilde{\Gamma}_s + \tilde{\Gamma}_s \hat{\chi}_0(\mathbf{p}) \tilde{\Gamma}_s \hat{\chi}_0(\mathbf{p}) \tilde{\Gamma}_s + \dots \\ &= \tilde{\Gamma}_s \hat{\chi}_0(\mathbf{p}) \tilde{\Gamma}_s [1 - \hat{\chi}_0(\mathbf{p}) \tilde{\Gamma}_s]^{-1} \end{aligned}$$

and

$$\begin{aligned} \tilde{V}_t^{lad}(\mathbf{k}, \mathbf{k}') &= \tilde{\Gamma}_t \hat{\chi}_0(\mathbf{p}) \tilde{\Gamma}_t + \tilde{\Gamma}_t \hat{\chi}_0(\mathbf{p}) \tilde{\Gamma}_t \hat{\chi}_0(\mathbf{p}) \tilde{\Gamma}_t + \dots \\ &= \tilde{\Gamma}_t \hat{\chi}_0(\mathbf{p}) \tilde{\Gamma}_t [1 - \hat{\chi}_0(\mathbf{p}) \tilde{\Gamma}_t]^{-1}, \end{aligned}$$

where $\mathbf{p} = \mathbf{k} + \mathbf{k}'$ and $\mathbf{q} = \mathbf{k} - \mathbf{k}'$, and the matrix \check{A} is related to matrix \hat{A} through the following relation,

$$\check{A}_{mn, m'n'} = \hat{A}_{nn', m'm}.$$

1. Matrix summation in the bubble diagrams

Below we write down the details on summing over the two series of matrices in the bubble diagrams,

$$\begin{aligned} \hat{A} &= \hat{\Gamma}_s - \hat{\Gamma}_s \hat{\chi}_0(\mathbf{q}) \hat{\Gamma}_t - \hat{\Gamma}_t \hat{\chi}_0(\mathbf{q}) \hat{\Gamma}_s \\ &\quad + \hat{\Gamma}_s \hat{\chi}_0(\mathbf{q}) \hat{\Gamma}_t \hat{\chi}_0(\mathbf{q}) \hat{\Gamma}_t + \hat{\Gamma}_t \hat{\chi}_0(\mathbf{q}) \hat{\Gamma}_s \hat{\chi}_0(\mathbf{q}) \hat{\Gamma}_t \\ &\quad + \hat{\Gamma}_t \hat{\chi}_0(\mathbf{q}) \hat{\Gamma}_t \hat{\chi}_0(\mathbf{q}) \hat{\Gamma}_s + \hat{\Gamma}_s \hat{\chi}_0(\mathbf{q}) \hat{\Gamma}_s \hat{\chi}_0(\mathbf{q}) \hat{\Gamma}_s + \dots \end{aligned}$$

and

$$\begin{aligned} \hat{B} &= \hat{\Gamma}_t - \hat{\Gamma}_s \hat{\chi}_0(\mathbf{q}) \hat{\Gamma}_s - \hat{\Gamma}_t \hat{\chi}_0(\mathbf{q}) \hat{\Gamma}_t \\ &\quad + \hat{\Gamma}_t \hat{\chi}_0(\mathbf{q}) \hat{\Gamma}_t \hat{\chi}_0(\mathbf{q}) \hat{\Gamma}_t + \hat{\Gamma}_t \hat{\chi}_0(\mathbf{q}) \hat{\Gamma}_s \hat{\chi}_0(\mathbf{q}) \hat{\Gamma}_s \\ &\quad + \hat{\Gamma}_s \hat{\chi}_0(\mathbf{q}) \hat{\Gamma}_t \hat{\chi}_0(\mathbf{q}) \hat{\Gamma}_s + \hat{\Gamma}_s \hat{\chi}_0(\mathbf{q}) \hat{\Gamma}_s \hat{\chi}_0(\mathbf{q}) \hat{\Gamma}_t + \dots \end{aligned}$$

where every term in \hat{A} contains odd number of $\hat{\Gamma}_s$ and every term in \hat{B} contains even number of $\hat{\Gamma}_s$, and each $\hat{\chi}_0$ contribute one minus sign. To do this summation, we multiple $\hat{\chi}_0(\mathbf{q})$ at both sides at first, then add them together or subtract one to another. Hence

$$\begin{aligned}\hat{\chi}_0(\mathbf{q})\hat{B} + \hat{\chi}_0(\mathbf{q})\hat{A} &= \hat{\chi}_0(\mathbf{q})(\hat{\Gamma}_t + \hat{\Gamma}_s) \\ &\quad \times [1 + \hat{\chi}_0(\mathbf{q})(\hat{\Gamma}_t + \hat{\Gamma}_s)]^{-1}, \\ \hat{\chi}_0(\mathbf{q})\hat{B} - \hat{\chi}_0(\mathbf{q})\hat{A} &= \hat{\chi}_0(\mathbf{q})(\hat{\Gamma}_t - \hat{\Gamma}_s) \\ &\quad \times [1 + \hat{\chi}_0(\mathbf{q})(\hat{\Gamma}_t - \hat{\Gamma}_s)]^{-1}.\end{aligned}$$

Then we obtain that

$$\begin{aligned}\hat{A} &= \frac{1}{2}(\hat{\Gamma}_t + \hat{\Gamma}_s)[1 + \hat{\chi}_0(\mathbf{q})(\hat{\Gamma}_t + \hat{\Gamma}_s)]^{-1} - \frac{1}{2}(\hat{\Gamma}_t \\ &\quad - \hat{\Gamma}_s)[1 + \hat{\chi}_0(\mathbf{q})(\hat{\Gamma}_t - \hat{\Gamma}_s)]^{-1}, \\ \hat{B} &= \frac{1}{2}(\hat{\Gamma}_t + \hat{\Gamma}_s)[1 + \hat{\chi}_0(\mathbf{q})(\hat{\Gamma}_t + \hat{\Gamma}_s)]^{-1} + \frac{1}{2}(\hat{\Gamma}_t \\ &\quad - \hat{\Gamma}_s)[1 + \hat{\chi}_0(\mathbf{q})(\hat{\Gamma}_t - \hat{\Gamma}_s)]^{-1}.\end{aligned}$$

-
- ¹ W. Wu, J. Cheng, K. Matsubayashi, P. Kong, F. Lin, C. Jin, N. Wang, Y. Uwatoko, and J. Luo, *Nat. Commun.* 5, 5508 (2014).
- ² Jin-Ke Bao, Ji-Yong Liu, Cong-Wei Ma, Zhi-Hao Meng, Zhang-Tu Tang, Yun-Lei Sun, Hui-Fei Zhai, Hao Jiang, Hua Bai, Chun-Mu Feng, Zhu-An Xu, Guang-Han Cao, *Phys. Rev. X* 5, 011013 (2015).
- ³ Zhang-Tu Tang, Jin-Ke Bao, Yi Liu, Yun-Lei Sun, Abduweli Ablimit, Hui-Fei Zhai, Hao Jiang, Chun-Mu Feng, Zhu-An Xu, Guang-Han Cao, *Phys. Rev. B* 91, 020506(R) (2015).
- ⁴ Zhang-Tu Tang, Jin-Ke Bao, Zhen Wang, Hua Bai, Hao Jiang, Yi Liu, Hui-Fei Zhai, Chun-Mu Feng, Zhu-An Xu, Guang-Han Cao, *Science China Materials*, 58(1), 16-10 (2015).
- ⁵ H. Z. Zhi, T. Imai, F. L. Ning, Jin-Ke Bao, Guang-Han Cao, *Phys. Rev. Lett.* 114, 147004 (2015).
- ⁶ G. M. Pang, M. Smidman, W. B. Jiang, J. K. Bao, Z. F. Weng, Y. F. Wang, L. Jiao, J. L. Zhang, G. H. Cao, H. Q. Yuan, *Phys. Rev. B* 91, 220502(R) (2015).
- ⁷ Hao Jiang, Guanghan Cao, Chao Cao, *Scientific Reports* 5, 16054 (2015).
- ⁸ Xianxin Wu, Congcong Le, Jing Yuan, Heng Fan, Jiangping Hu, *Chin. Phys. Lett.* 32,057401(2015)
- ⁹ Tai Kong, Sergey L. Bud'ko, Paul C. Canfield, *Phys. Rev. B* 91, 020507 (2015) .
- ¹⁰ P. H. Butler, Point Group Symmetry Applications: Methods and Tables, Plenum Press, New York (1981).
- ¹¹ D. J. Scalapino, E. Loh, Jr., and J. E. Hirsch, *Phys. Rev. B* 35, 6694 (1987).
- ¹² In private communication with Daniel F. Agterberg, we learnt that he had a smiliar table as ours.
- ¹³ Patrick A. Lee and Xiao-Gang Wen, *Phys. Rev. B* 78, 144517 (2008).